Miktoarm Stars via Grafting-Through Copolymerization: Self-Assembly and the Star-to-Bottlebrush Transition

Adam E. Levi[†|], Joshua Lequieu[‡|], Jacob D. Horne[§], Morgan W. Bates[‡], Jing M. Ren[‡], Kris T. Delaney[‡], Glenn H. Fredrickson[‡§⊥], and Christopher M. Bates[⊥§‡*]

[†]*Department of Chemistry and Biochemistry,* [‡]*Materials Research Laboratory*, [§]*Department of Chemical Engineering, and* [⊥]*Materials Department, University of California, Santa Barbara, California 93106, United States.*

[|]*These authors contributed equally*

Keywords: bottlebrush, miktoarm star, polyester, star transition, macromonomer, grafting-through polymerization, ring opening metathesis polymerization

GRAPHICAL TABLE OF CONTENTS

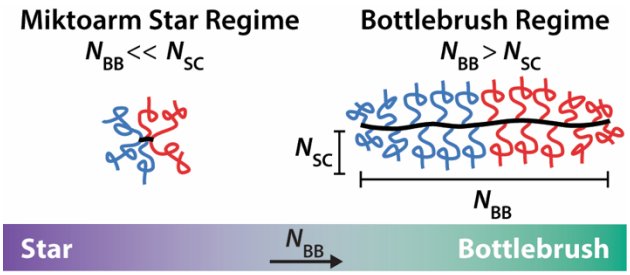

ABSTRACT

The grafting-through copolymerization of two distinct macromonomers via ring-opening metathesis polymerization is typically used to form statistical or diblock bottlebrush polymers with large total backbone degrees of polymerization (N_{BB}) relative to that of the side-chains (N_{SC}). Here, we demonstrate that Grubbs-type chemistry in the opposite limit, namely $N_{BB} << N_{SC}$, produces well-defined materials with excellent control over ensemble-averaged properties, including molar mass, dispersity, composition, and number of branch points. The dependence of self-assembly on these molecular design parameters was systematically probed using small angle X-ray scattering and self-consistent field theoretic simulations. Our analysis supports the notion that two-

component bottlebrush copolymers with small N_{BB} behave like miktoarm star polymers. The star-to-bottlebrush transition is quantifiable for both statistical and diblock sequences by unique signatures in the experimental scaling of domain spacing and simulated distribution of backbone/side-chain density within lamellar unit cells. These findings represent a conceptual framework that simplifies the synthesis of miktoarm star polymers when dispersity in the number of arms and composition can be tolerated. The analytical approach introduced to distinguish chain conformations in complex macromolecules also complements previous methods, for example form factor scattering and rheology.

INTRODUCTION

Block polymers are important in fundamental[1–3] and applied[4–6] research due to their synthetic tractability, facile processing, and unique self-assembly. A wealth of experimental and theoretical methods are now available to create materials with prescribed control over desired properties spanning molecular to macroscopic length scales. One design parameter with powerful potential is the careful placement of branching. For example, bottlebrush polymers (Figure 1a) are characterized by a long polymeric backbone with additional polymeric side-chains protruding off of many or all repeat units.[7] The steric congestion encoded by this connectivity tends to elongate backbone conformations, providing value for applications including photonics,[8,9] electrochemical devices,[10] dielectric elastomers,[11] lithography,[12,13] giant surfactants,[14] and drug delivery.[15,16] Miktoarm star polymers (Figure 1b) are another type of branched macromolecule characterized by chemically-distinct chains connected at a common junction.[17] Asymmetry in arm type (e.g., A_mB_n, $m \neq n$) significantly perturbs the traditional two-component block copolymer phase diagram, with consequences for contemporary topics like complex phase behavior[18] and thermoplastic

elastomers.[19] The opportunities afforded by branched block polymers are only beginning to emerge.

Despite the many advantageous properties of branched block polymers, traditional synthetic strategies can be laborious. Discrete miktoarm stars typically require a complicated series of convergent or divergent chemical manipulations to build.[20] While possible using various (de)protection and controlled polymerization methodologies, any extensive exploration of the vast design space that underpins exquisite material performance is often infeasible. In contrast, bottlebrushes with 100% grafting density (one side-chain per backbone repeat unit) are actually relatively easy to access via grafting-through polymerization of end-reactive monotelechelic macromonomer precursors.

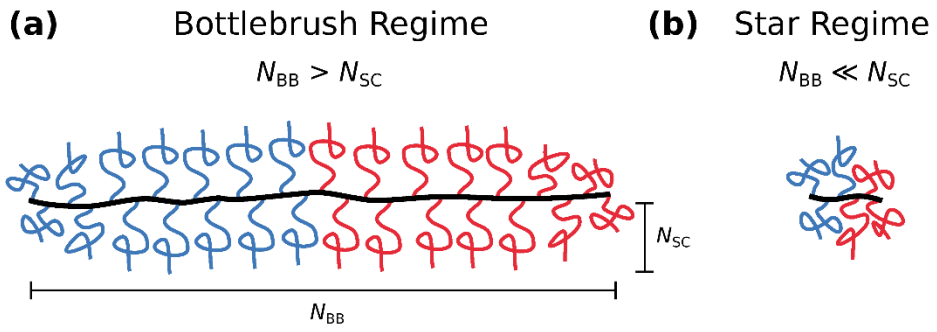

Figure 1. A densely grafted copolymer in two limits of backbone and side-chain length. **(a)** Bottlebrush ($N_{BB} >> N_{SC}$), and **(b)** miktoarm star ($N_{BB} << N_{SC}$).

Motivated by the challenge to construct well-defined miktoarm star polymers in a simple and versatile fashion, here we exploit the benefits of grafting-through copolymerization and demonstrate that it generates hetero-arm stars in the limit of short total backbone degrees of polymerization (N_{BB}) with sufficiently long side-chain degrees of polymerization (N_{SC}). Small angle X-ray scattering and self-consistent field theoretic (SCFT) simulations reveal three distinguishable regimes of self-assembly that we relate to chain conformations straddling: (I)

compositional dispersity-dominated behavior at low N_{BB}, (II) a star-to-bottlebrush transition regime, and (III) bottlebrush. The specific details of this star-to-bottlebrush crossover are a function of N_{BB}, N_{SC}, and macromonomer sequence (diblock vs. statistical). As described below, these insights into the self-assembly of miktoarm star polymers containing molar mass and compositional dispersity (arising from macromonomer copolymerization) strengthen our fundamental understanding of this exciting material platform.

RESULTS AND DISCUSSION

Synthesis and Self-assembly

Norbornene-terminated macromonomers (MM) of poly(lactide) (PLA) and poly(4-methyl-ε-caprolactone) (P4MCL) were prepared via ring-opening transesterification polymerization as described in the Methods section and Supporting Information (Schemes S1–S2). Two molar masses were synthesized for each: PLA-MM-3.3 = 3.3 kg mol^{-1}, PLA-MM-12 = 12 kg mol^{-1}, P4MCL-MM-3.7 = 3.7 kg mol^{-1}, and P4MCL-MM-11 = 11 kg mol^{-1}, all of which exhibit unimodal molar mass distributions (Figure S1) and reasonable dispersities ($Đ \leq 1.11$, Table S1). These macromonomers were then subjected to ring-opening metathesis copolymerization (ROMP) using a Grubbs third generation bis-pyridine derivative[21] (G3) in two ways: (1) with sequential addition ("block", Scheme S3), and (2) from a preformed mixture that results in statistical incorporation ("statistical", Scheme S4). Statistical and diblock copolymers prepared from PLA-MM-12 and P4MCL-MM-11 are hereafter denoted as the S12 and B12 series, respectively. Likewise, PLA-MM-3.3 and P4MCL-MM-3.7 were copolymerized to generate two series called S3 and B3. We will collectively refer to these materials as "bottlebrush polymers," although as substantiated later, shorter variants are more appropriately termed miktoarm stars. Figure 2 reports

selected size-exclusion chromatograms for B12 (Figure 2a) and S12 (Figure 2b) copolymers with near-symmetric compositions (volume fractions f_{PLA} = 0.48 ± 0.01) at different backbone degrees of polymerization (as measured with multi-angle light scattering size-exclusion chromatography). Tables S2–S5 and Figures S2–S11 summarize the pertinent bottlebrush polymer characterization data.

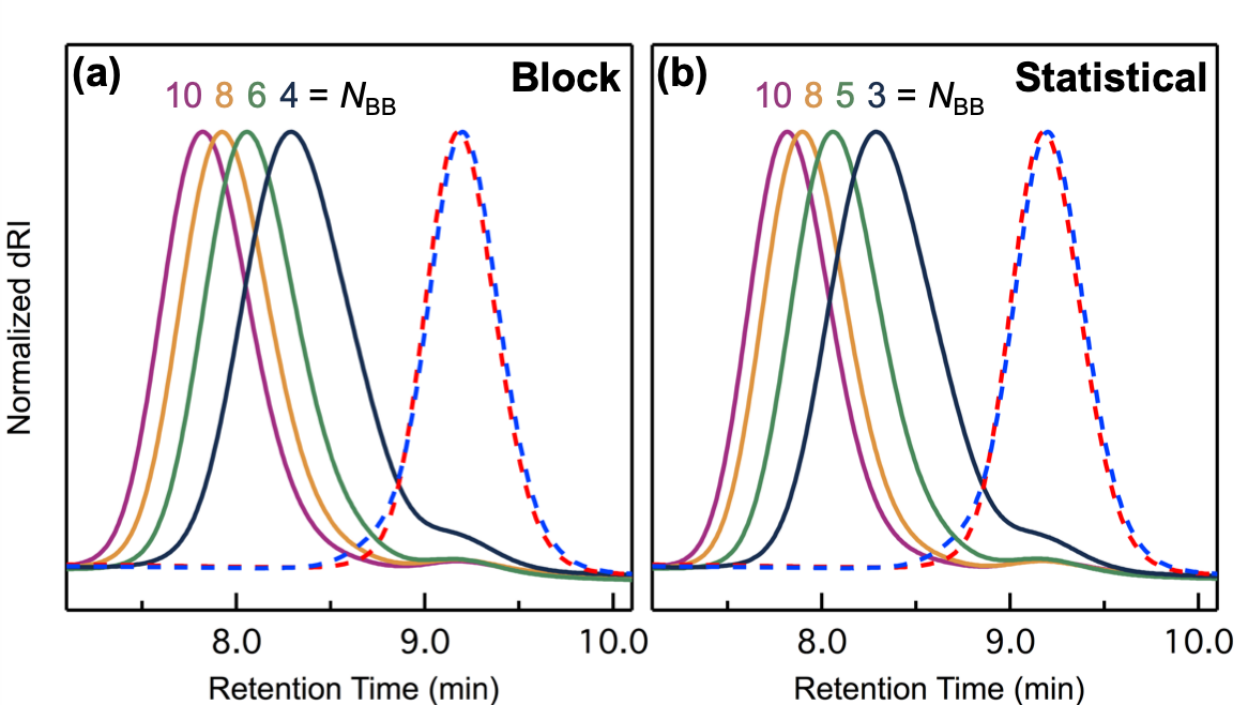

Figure 2. Normalized size-exclusion chromatograms (differential refractive index detection) of low-N_{BB} bottlebrush copolymers with 12 kg mol^{-1} PLA (PLA-MM-12) and 11 kg mol^{-1} P4MCL (P4MCL-MM-11) side-chains. PLA and P4MCL macromonomers are shown in red and blue dashed lines, respectively. Sequence: **(a)** block, **(b)** statistical. The small bump near 9.2 min is residual macromonomer (< 3% by area in all samples).

The bottlebrush polymers were first studied using synchrotron small angle X-ray scattering (SAXS) to interrogate bulk self-assembly. Both the B12 and S12 series form well-ordered nanostructures that exhibit Bragg reflections (q/q^* = 1, 2, 3, 4, 5, …) consistent with lamellar

periodicity (Figure 3).[22] Remarkably, even samples with N_{BB} = 3 display higher order peaks. In contrast, lower molar mass samples ($N_{BB} \lesssim 9$) from B3 and S3 with shorter side-chains do not order at small N_{BB} as a result of the moderate Flory–Huggins interaction parameter between PLA and P4MCL — χ = 0.10 at 298 K with a 118 Å^3 reference volume.[23] (Correlation–hole scattering is evident, see Figures S4a, S7a.) Sharper primary peaks and the emergence of secondary peaks when $N_{BB} \gtrsim 10$ suggest a transformation to ordered nanostructures although definitive morphological assignment remains inconclusive in the absence of a sufficient number of reflections. We suspect that these samples are still lamellar based on their volume fractions and proximity in phase space to those described in Figure 3.

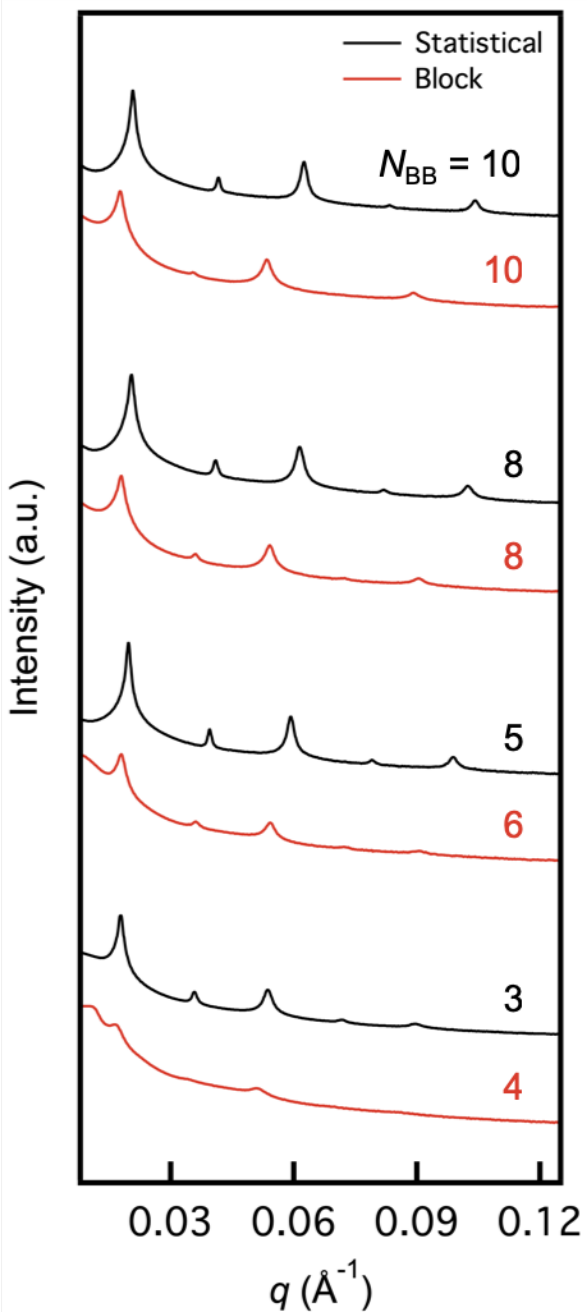

Figure 3. SAXS patterns (log intensity vs. q) of samples S12 (red, N_{BB} = 3, 5, 8, 10) and B12 (black, N_{BB} = 4, 6, 8, 10). All Bragg reflections (q/q^* = 1, 2, 3, 4, 5, …) are consistent with lamellar periodicity.[22]

Scaling Trends

Characteristic domain spacings $d^* = 2\pi/q^*$ were extracted from principal scattering peaks (q^*) and plotted against N_{BB} (Figure 4a). Three qualitatively-distinct scaling regimes are evident in each experimental dataset: (I) a shallow but significant decrease in d^* (approximately 3 to 4 nm) as N_{BB} increases at small N_{BB} (circa ≤ 6), (II) an intermediate transition with a weak dependence ($6 < N_{BB} \leq 15$), and (III) a region of constant slope (either increasing or flat) at large N_{BB} (roughly > 15). The last limit (regime III, $N_{BB} \to \infty$) is consistent with previous experiments[24–26] that rationalize the dissimilar dependence of $d^* \sim N_{BB}^{\alpha}$ for statistical ($\alpha \approx 0$) and block ($0 << \alpha < 1$) sequences by different orientations of the bottlebrush backbone — approximately parallel or perpendicular to the lamellar interface, respectively. The remainder of this manuscript focuses on the behavior at smaller N_{BB} that is less well-understood.

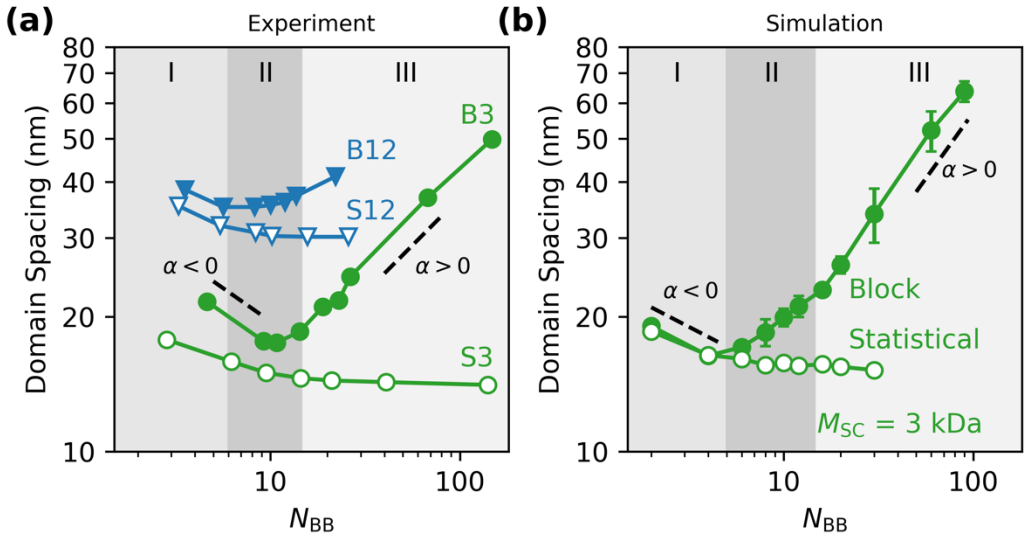

Figure 4. Log–log plot of lamellar domain spacing versus N_{BB} for bottlebrush copolymers comprising statistical (open symbols) and blocky (closed symbols) sequences. **(a)** Experimental SAXS data for B3/S3 (green) and B12/S12 (blue). **(b)** SCFT-predicted domain spacing with composition and arm number dispersity for $M_{SC} = 3$ kg mol^{-1}. The scaling exponent α in region

III is 0.4 and 0.6 for the experimental and SCFT data, respectively.

For the shortest backbone lengths (regime I), we attribute the decrease in d^* with increasing N_{BB} ($\alpha < 0$) to dispersity effects that arise from the unavoidable distribution in composition and number of arms inherent to the ROMP copolymerization of two homopolymer macromonomers. SCFT calculations (Figure S12–S15, Eqns. S1–S14) of block bottlebrushes in the absence of dispersity fail to capture the experimental trend and instead predict a monotonic increase in d^* with N_{BB} (Figure S13). In contrast, simulations conducted with a variety of different chains varying in their number of arms and composition (see Methods and Supporting Information) reveals qualitatively similar curves (Figure 4b) as experiments (Figure 4a) at all N_{BB} for ≈ 3 kg mol^{-1} side-chains with statistical and blocky sequences. While the best agreement between simulation and experiment is obtained by including both types of dispersity, compositional dispersity is the most significant (Figure S13). The signature of each experimental scaling regime is recovered, in particular the negative slope for small N_{BB}. This effect appears to originate from an appreciable concentration of homopolymer bottlebrushes that form due to compositional dispersity, which swell the lamellae and dilate domain periodicity. Since probability biases more homopolymer at short average backbone degrees of polymerization, as N_{BB} reaches 20 repeat units, the aforementioned scaling (regime III) is essentially unaffected by such dispersity and α asymptotes. Together, these results indicate that dispersity, and especially compositional dispersity, play an important role in the self-assembly of short bottlebrush polymers synthesized via grafting-through copolymerization.

One might anticipate that regime II, the region of intermediate scaling, is indicative of a transition from star-like to bottlebrush-like conformations as N_{BB} grows. The approximate plateau in d^* (which is readily apparent in the B12 block sequence) would then be consistent with two

competing effects: (1) fewer homopolymers and less swelling, which together decrease domain spacing with increasing N_{BB}, and (2) the star-to-bottlebrush transition that results from an amplification of steric congestion surrounding the elongating backbone, extending chain configurations and raising d^*.

Figure 5 illustrates the key characteristics of regimes I, II, and III. We are particularly interested in understanding the transition region (II) in more detail since it distinguishes well-established bottlebrush behavior from the miktoarm star materials of interest. Because this is difficult with experiments, we instead develop a more detailed SCFT analysis to clarify the location of the miktoarm star-to-bottlebrush crossover.

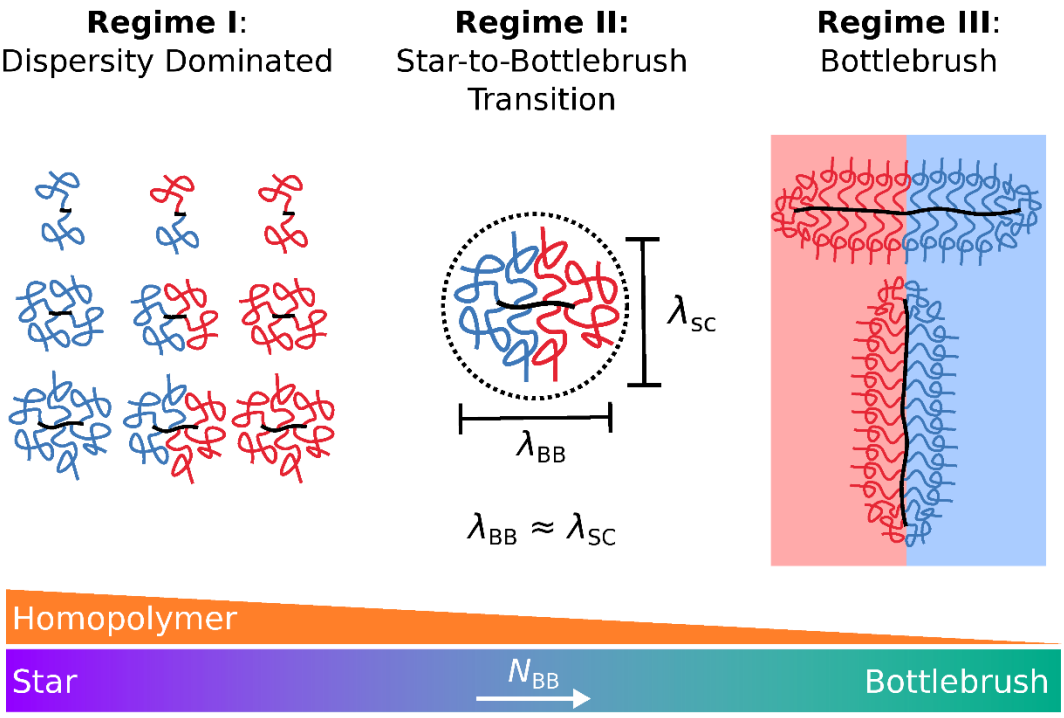

Figure 5. Illustrations describing the factors that control scaling ($d^* \sim N_{BB}^{\alpha}$) in the three regimes observed with two-component bottlebrush copolymers. **(a)** Small N_{BB}: dispersity in the number of arms and composition results in $\alpha < 0$. **(b)** Moderate N_{BB}: chain conformations transition from miktoarm star to bottlebrush when backbone (λ_{BB}) and side-chain extensions (λ_{SC}) become

comparable as the concentration of homopolymers tapers off; $\alpha \gtrsim 0$. **(c)** Large N_{BB}: backbone orientation depends on sequence (consistent with prior experiments[24] and the SCFT simulations reported herein.)

Miktoarm Star-to-Bottlebrush Transition

To elucidate the details of the miktoarm star-to-bottlebrush transition using SCFT, we begin by examining the effect of backbone length on the domain spacing of block bottlebrush copolymers in the absence of dispersity, which allows us to decouple the competing effects of homopolymer-induced swelling and backbone elongation that characterize the intermediate scaling regime II. When dispersity is removed from our SCFT calculations (Figure 6), only two regimes are observed: one at large N_{BB} corresponding to rapidly increasing domain spacing (III′) and another at low N_{BB} corresponding to slower domain spacing growth (II′). As noted previously by Dalsin et al.,[26] this decrease in α is attributed to the onset of miktoarm-star-like behavior. We denote the crossover between regimes II′ and III′ by N_{BB}*, e.g., N_{BB}* ≈ 12 for 3 kg mol^{-1} side-chains. This value corresponds well with the experimentally observed transition from the large N_{BB} regime III to the intermediate N_{BB} regime II that falls somewhere around N_{BB} = 12 (Figure 4a).

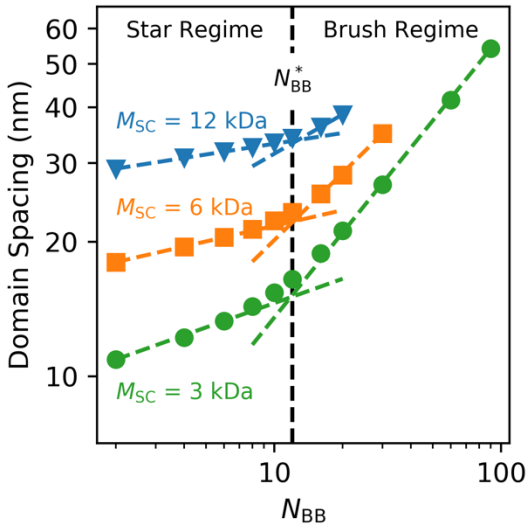

Figure 6. SCFT calculations of block bottlebrush copolymer domain spacing as a function of backbone length N_{BB}. Different colors denote side-chain lengths of M_{SC} = 3, 6, and 12 kg mol^{-1}. The change in slope occurs at N_{BB}*, which is nearly constant for all simulated side-chain lengths.

For larger 6 and 12 kg mol^{-1} side-chains, the bottlebrushes exhibit a weaker dependence of domain spacing on N_{BB} as indicated by lower values of α across the whole range (regimes II′ and III′). This is consistent with our experimental results comparing 3 and 12 kg mol^{-1} side-chains (Figure 4a) and suggests that larger side-chains lead to slightly more flexible backbones at the values of N_{BB} probed. Nevertheless, despite their lower values of α, the bottlebrushes with M_{SC} = 6 and 12 kg mol^{-1} also exhibit two scaling regimes at low and high N_{BB}, again with a crossover at N_{BB}*. Remarkably, the value of N_{BB}* is approximately constant for all side-chain lengths commensurate with experiments, M_{SC} = 3, 6, and 12 kg mol^{-1} (Figure 6). Evidently, even for relatively short 3 kg mol^{-1} side-chains, the backbone stiffening due to steric repulsion is essentially saturated, thereby leading to a conserved star-to-bottlebrush transition at N_{BB}* = 12. Additional simulations indicate that N_{BB}* will decrease with shorter 1.5 kg mol^{-1} side-chains (Figure S14a), and it is also very slightly dependent on the segregation strength χN_{SC} (Figure S14b). The

independence of N_{BB}* with most M_{SC} predicted by SCFT is consistent with our experimental data; although it is difficult to precisely pinpoint N_{BB}* in Figure 4a due to the effects of dispersity, N_{BB}* = 12 nonetheless appears to be the approximate location of the change in α scaling for both 3 and 12 kg/mol side-chains. As demonstrated, SCFT predictions of domain spacing are useful for identifying N_{BB}* with block bottlebrushes and comparing model predictions with experiments, but this analysis does little to explain the molecular origin of the shift in α at $N_{BB} = N_{BB}$*. We next turn to different SCFT calculations to assess this aspect of the star-to-bottlebrush transition.

Molecular Explanation of the Miktoarm Star-to-Bottlebrush Transition

One molecular signature of the star-to-bottlebrush transition is a change in backbone conformation as a function of N_{BB} *with the block sequence*. Figure 7a shows simulated backbone density profiles for monodisperse samples with N_{BB} = 6, 12 and 30 and M_{SC} = 3 kg mol^{-1}. When N_{BB} is large (regime III, e.g., N_{BB} = 30), the backbone conformations of statistical and block bottlebrushes exhibit large differences. Statistical brushes orient their backbones parallel to the lamellar interface, which leads to a density profile that is strongly peaked at $x/L_0 = 0.5$, where x is the position within a unit cell and L_0 is the natural periodicity. In contrast, block bottlebrush backbones preferentially orient perpendicular to the interface, thereby smearing out the density profile across a lamellar unit cell. (These data are consistent with the illustrations in Figure 5c and prior experimental literature.[24–26]) However, such sequence effects become nearly indistinguishable as N_{BB} decreases. For a short bottlebrush with N_{BB} = 6, block and statistical backbone distributions are essentially identical, with both density profiles strongly peaked at the lamellar interface (Figure 7; see also Figure S15). The independence of backbone distribution on side-chain arrangement at low N_{BB} indicates that the backbone has no preferred orientation within

the lamellar interface. Intermediate backbone lengths corresponding to $N_{BB} = N_{BB}^* = 12$ exhibit a density profile that is mixed between these two extremes; the density is peaked at the interface, but there is still appreciable backbone density within the interior of lamellar domains. This finding suggests that the configuration of a *block* bottlebrush backbone can be used as a hallmark of the star-to-bottlebrush transition: when the backbone of a *block* bottlebrush begins to localize near the domain interface, it starts to behave like a star.

To quantify this transition in greater detail, we examine the probability of finding a bottlebrush backbone at the domain interface, $P_{interface}$, as a function of N_{BB} (Figures 7b; see Methods). For statistical bottlebrushes, this probability is approximately constant for $N_{BB} > N_{BB}^*$ before increasing at small backbone lengths. Note that this implies the statistical sequence does undergo a small change in backbone distribution as a function of N_{BB}, but the effect is rather minimal. In contrast, the probability for block sequences is highly variable; it is approximately zero when $N_{BB} > 20$, before increasing for smaller N_{BB}. Notably, what we have previously defined as $N_{BB}^* = 12$ corresponds roughly to the onset of this dramatic backbone redistribution. Consistent with our observation in Figure 6, changing M_{SC} from 3 to 12 kg mol^{-1} has little effect on backbone localization to the interface as measured by $P_{interface}$.

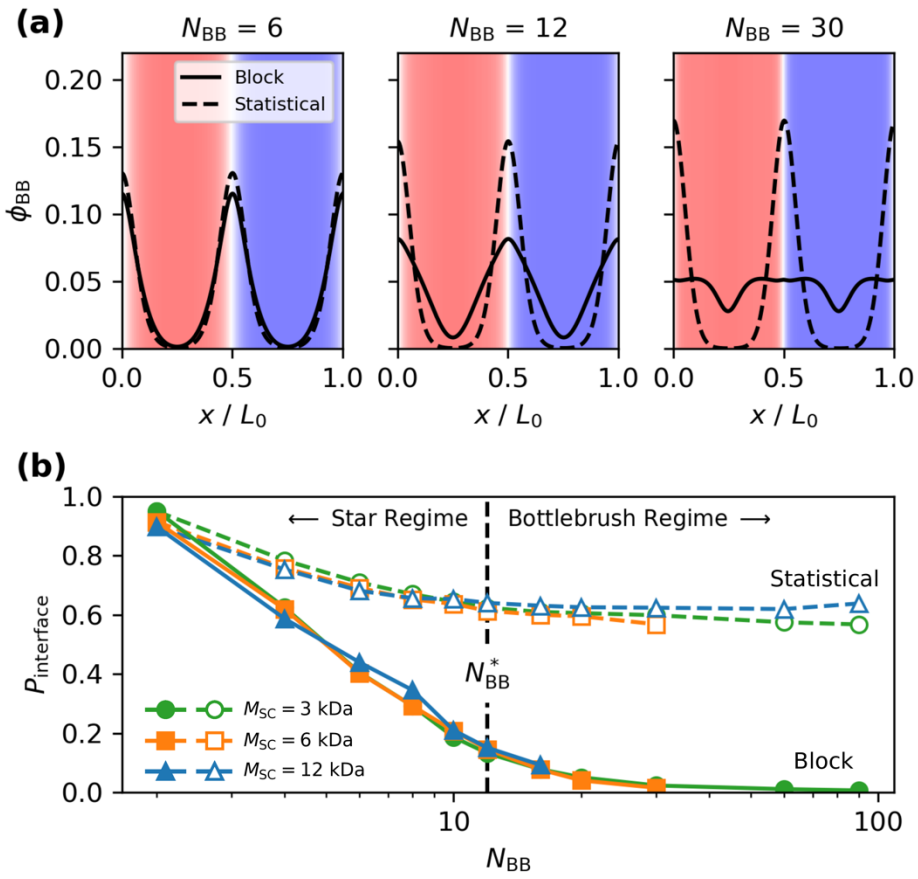

Figure 7. (a) SCFT calculations of backbone segment distribution, ϕ_{BB}, across a lamellar period with statistical and block macromonomer sequences (M_{SC} = 3 kDa) for N_{BB} = 6, N_{BB} = 12 (= N_{BB}*), and N_{BB} = 30. The red, blue, and white shading indicates PLA-rich domains, P4MCL-rich domains, and the interface, respectively. x denotes the position within a lamellar unit cell and L_0 is the domain periodicity. **(b)** Probability of backbone localization at the interface, $P_{interface}$, for different N_{BB} and M_{SC}.

Taken together, these results offer a molecular explanation for the scaling regimes II and III observed in Figures 4 and 6. For $N_{BB} > N_{BB}$*, the backbone extension is large relative to the interface, and domain spacing scales strongly with N_{BB}. In contrast when $N_{BB} < N_{BB}$*, the backbone extension is comparable to the interface width, leading to localization of the backbone at the

interface and signaling increasingly miktoarm-star-like behavior. Experimental measurements of domain-spacing versus N_{BB} thus provide an excellent metric for identifying this molecular transition, specifically with *block* bottlebrush copolymers.

Miktoarm Star-to-Bottlebrush Transition in Statistical Copolymers

Since statistical bottlebrushes undergo a comparably modest backbone redistribution as a function of N_{BB}, the analysis described in Figure 7 cannot similarly be used as a proxy to interrogate their star-to-bottlebrush crossover. Clear signatures of the star-to-bottlebrush transition with the statistical sequence are also absent from the experimental data in Figure 4a, so the analysis presented up to now cannot examine the role that macromonomer sequence (i.e., block vs. statistical) plays in the star-to-bottlebrush transition. In order to probe sequence effects in more detail, it was necessary to compute the relative extension of the bottlebrush backbone (λ_{BB}) and side-chains (λ_{SC}) (see Methods). Once these lengths were determined, we define a dimensionless quantity $\lambda_{BB}/\lambda_{SC}$ that describes the aspect ratio of a given bottlebrush polymer. For $\lambda_{BB}/\lambda_{SC} \gg 1$, a bottlebrush is highly elongated and the molecules are expected to adopt more cylindrical-like configurations. In contrast, for $\lambda_{BB}/\lambda_{SC} \ll 1$, the backbone is vanishingly small and bottlebrush polymers should instead mimic spherical or star-like objects. The star-to-bottlebrush transition is then expected to occur circa $\lambda_{BB}/\lambda_{SC} \approx 1$. If our prior analysis is robust, this crossover will correspond with N_{BB}* as identified above.

We therefore used SCFT simulations to compute $\lambda_{BB}/\lambda_{SC}$ for both sequences (statistical and block) with varying N_{BB} and identified the value at which $\lambda_{BB}/\lambda_{SC} = 1$ (Figure 8). In both cases, $\lambda_{BB}/\lambda_{SC} = 1$ at similar values of N_{BB} (8 for block, 14 for statistical). For block bottlebrushes, the previously identified value of N_{BB}* = 12 correlates quite well with $\lambda_{BB}/\lambda_{SC} \approx$

1, indicating that $\lambda_{BB}/\lambda_{SC}$ is a suitable metric for establishing the location of a star-to-bottlebrush transition. This result has two important consequences. First, the correspondence between N_{BB}* and $\lambda_{BB}/\lambda_{SC} = 1$ provides an additional physical explanation for the star-to-bottlebrush transition — it suggests that the change in slope at N_{BB}* can be correctly thought of as the point when a bottlebrush molecule transitions from a cylindrical-like to a spherical object. Second, the consistent picture that emerges from our different analyses of the block sequence, coupled with similar values of N_{BB} for $(\lambda_{BB}/\lambda_{SC})_{block} = 1$ and $(\lambda_{BB}/\lambda_{SC})_{statistical} = 1$, allows us to posit that the star-to-bottlebrush transition is largely independent of sequence. Both block and statistical copolymers seem to transition at almost equivalent backbone lengths. There may be a slightly earlier transition for the block sequence due to a small bias for stiffer backbones, but this effect is modest.

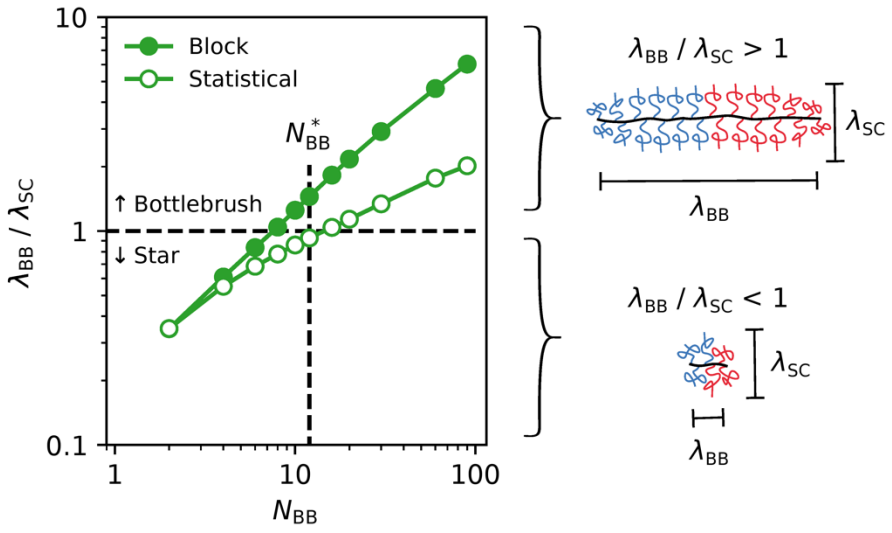

Figure 8. Calculated bottlebrush aspect ratio ($\lambda_{BB}/\lambda_{SC}$) for block and statistical macromonomer sequences with M_{SC} = 3 kg mol^{-1}. The value of N_{BB} where $\lambda_{BB}/\lambda_{SC} \approx 1$ corresponds well with the value of N_{BB}* obtained from the domain spacing analysis in Figure 6.

Discussion

The virtues of ring-opening metathesis polymerization are now well-known and have ushered in an era of synthetic simplicity that has changed the accessibility of cutting-edge materials for numerous applications.[8–16] Major efforts by Bowden,[27,28] Wooley,[29,30] and Grubbs[31–33] have adapted ROMP to construct bottlebrush polymers ($N_{BB} >> N_{SC}$) with amazing control over molar mass and dispersity. Less attention has been devoted to exploiting this versatile chemistry in the opposite limit, $N_{BB} < N_{SC}$. In the context of *bulk* phase behavior, although a few reports[26,34] include samples with $N_{BB} < N_{SC}$, efforts have not focused heavily on this regime. Here, we have demonstrated that the sequential or statistical grafting-through copolymerization of two macromonomers with $N_{BB} < N_{SC}$ results in materials that self-assemble into well-ordered lamellar structures. While we have not yet attempted to do so, there are no fundamental limitations that prevent the extension of this approach to other, more complex, design targets — for example, ≥ 3 distinct chemistries and multiblock side-chains[29,30] or sequences.[10] Synthesizing miktoarm star polymers with the present technique affords a number of advantages that revolve around versatility. The *average* number of arms and composition are easily manipulated by stoichiometry, but of course, the price paid is dispersity in both. (Since ring-opening transesterification polymerization and ROMP are controlled, the unavoidable dispersity in molar mass is similar to other miktoarm star polymerization strategies.) These distributions could be either a benefit[35] or burden[36] depending on perspective. Either way, we have systematically studied their effect in the context of self-assembly and chain conformations. Finally, as a tangential observation, the dispersity accompanying our approach seems to counteract the phase boundary deflection that is characteristic of asymmetric (in connectivity) miktoarm star polymers.[37] For example, Grason has previously predicted[38] and Tselikas observed[39] hexagonally-packed cylinder phases at roughly

symmetric volume fractions $f_A \approx 0.5$ in an AB_3 miktoarm star polymer. Herein, samples synthesized near this composition with a 1:3 ratio of A:B side-chains are decidedly lamellar (Figure S9–S11).

Johnson and coworkers have pioneered the use of ROMP to construct "core-crosslinked" molecules termed "mikto-brush-arm star polymers"[40–42] that bear some similarities to the materials described herein. Their synthetic method also leverages the benefits of ROMP to build arms via macromonomer copolymerization. The key distinction is a final step involving the addition of multi-functional norbornene crosslinker, which forms a compact core that polymerized macromonomers protrude from. Such core-crosslinking has undoubtedly proven useful in a variety of applications[42–49] but the molecular connectivity is fundamentally different compared to low-N_{BB} statistical and block bottlebrush polymers. No crosslinking step is involved in our approach and the core of each star polymer is precisely the well-defined poly(norbornene) backbone that is formed during ROMP in the absence multi-functional additives.

The star-to-bottlebrush transition has been investigated in other material systems, many of which employed just one type of side-chain chemistry. A recent report analyzed atactic poly(propylene) bottlebrush polymer melts with varying degrees of polymerization and concluded, based on zero-shear viscosity data, that the star-to-bottlebrush change in chain conformation likely occurs over the range $N_{BB} = 26–74$.[50] Small angle neutron scattering measurements of polystyrene bottlebrush side-chains in a good solvent place the transition somewhere around $N_{BB} = 120$.[51] We speculate that these numbers are larger than those ascertained here due to differences in the free energy of two- and one-component polymers. As described in Figures 4–8, the transition from bottlebrush-to-star conformations for bottlebrush *co*polymers occurs when N_{BB} decreases towards 12. With the block sequence, this value marks the beginning of backbone unalignment so that it

resides at the lamellar interface with no favored orientation. However, this transformation is presumably quite difficult if the backbone cannot occupy a tight region of space around the interface; otherwise, the system would be forced to create enthalpically-unfavorable contacts between the two different types of side-chains. From the present analysis, $\lesssim$12 repeat units is apparently sufficient to overcome this energetic dichotomy, but the thermodynamic landscape would undoubtedly change without such constraints (e.g., homopolymer bottlebrushes).

A transition reminiscent of the star-to-bottlebrush crossover has also been observed in polymers produced from branched macromonomers containing both poly(styrene) and poly(dimethylsiloxane) (PDMS) side-chains.[34] Note that the composition dispersity inherent to statistical ROMP *co*polymerization can be suppressed using this approach, but the homopolymerization of diblock macromonomers eliminates control over the average number of each arm type — the resulting star or bottlebrush materials are necessarily A_nB_n. Nevertheless, in this case, the monotonic increase in domain spacing observed for samples with increasing N_{BB} ($\lesssim$ 10) is believed to originate from chain stretching effects that saturate at modest backbone lengths. These data support our conclusion that compositional dispersity dominates the d^* vs. N_{BB} scaling ($\alpha < 0$) observed in Figure 4 (regime I). In analogy to recent work from Zhong,[52] the impact of compositional dispersity on additional physical properties would also be interesting to probe, for example the glass transition temperature, order–disorder temperature, and storage modulus.

Finally, we draw comparisons to another paper by Dalsin et al.[26] that studied bottlebrush block polymers comprising atactic poly(propylene) and poly(styrene) side-chains. They identified a decrease in the scaling exponent ($\alpha = 0.26$) between N_{BB} = 10–15 and attributed it to "starlike" molecules. These samples lie beyond the N_{BB} boundary (II–III) that we observe as the onset of star-like behavior. By extending the scaling analysis to even smaller N_{BB}, we have uncovered the

limiting behavior of α, which further transforms d^* into a minimum and then dips negative. A second key conclusion from their paper is the assertion that bottlebrush backbones are actually significantly more flexible than commonly believed. Our evidence also seems to support this notion. As shown in Figure 4a, the domain spacing of PLA–P4MCL bottlebrush block copolymers expands by a factor of 1.5–2 when side-chain molar mass increases from 3 to 12 kg mol^{-1}. This result is inconsistent with the traditional interpretation of block bottlebrushes as rigid cylindrical objects always oriented perpendicular to the domain interface. If side-chains only extended parallel to the interface, domain spacing would not (or only weakly) depend on their length. Instead, our data is consistent with the conclusion that a backbone is strongly oriented near the interface, but this order decays with distance, eventually allowing side-chains to influence domain spacing.[26]

CONCLUSION

We have demonstrated that the grafting-through ring-opening metathesis polymerization of two macromonomers with a statistical or blocky sequence generates miktoarm star polymers in the low backbone degree of polymerization limit ($N_{BB} < N_{SC}$). A series of symmetric volume fraction ($f_{PLA} \approx 0.5$) materials with poly(lactide) and poly(4-methyl-ε-caprolactone) side-chains (≈3 or 12 kg mol^{-1}) self-assemble into lamellar structures with a characteristic domain spacing that strongly depends on N_{BB}. Using these trends in conjunction with self-consistent field theoretic simulations, three scaling regimes were identified that are distinguished as: (I) dispersity-dominated, (II) a star-to-bottlebrush transition, and (III) bottlebrush. SCFT calculations have revealed that the miktoarm star-to-bottlebrush transition can be captured by analyzing the redistribution of backbone segments within a lamellar unit cell as a function of N_{BB} for the block sequence. The location of this transition occurs at approximately $N_{BB}^* = 12$ and is largely independent of side-chain length and macromonomer sequence. The synthetic strategy disclosed

herein significantly simplifies access to discrete miktoarm star polymers that organize into well-ordered mesostructures when dispersity in composition and the number of arms can be tolerated. These materials have provided insights into the interplay between dispersity, molecular conformations, and self-assembly.

AUTHOR INFORMATION

Corresponding Author

* cbates@ucsb.edu

Author Contributions

The manuscript was written by AEL, JL, and CMB. Experiments were designed by AEL and CMB and performed by AEL, JDH, MWB, and JMR. Simulations were designed by JL, KTD and GHF and performed by JL. All authors have given approval to the final version of the manuscript.

Funding Sources

This material is based upon work supported by the U.S. Department of Energy, Office of Basic Energy Sciences, under Award Number DE-SC0019001. AEL thanks the Mellichamp Academic Initiative in Sustainability for summer fellowships. The research reported here made use of shared facilities of the UCSB MRSEC (NSF DMR 1720256), a member of the Materials Research Facilities Network (www.mrfn.org).

Notes

The authors declare no competing financial interest.

ACKNOWLEDGMENTS

The authors thank Craig J. Hawker and his group for intellectual discussions, Rachel Segalman for dRI SEC data, and William Wolf for help with SEC-MALS. Portions of this work were performed at the DuPont-Northwestern-Dow Collaborative Access Team (DND-CAT)

located at Sector 5 of the Advanced Photon Source (APS). DND-CAT is supported by Northwestern University, E.I. DuPont de Nemours & Co., and The Dow Chemical Company. This research used resources of the Advanced Photon Source, a U.S. Department of Energy (DOE) Office of Science User Facility operated for the DOE Office of Science by Argonne National Laboratory under Contract No. DE-AC02-06CH11357. Data was collected using an instrument funded by the National Science Foundation under Award Number 0960140.

Methods

Synthesis

Full synthetic methods are provided in the Supporting Information, including purification, small molecule and polymer synthesis, and characterization data.

Characterization

Multi-angle light scattering size-exclusive chromatography (SEC-MALS) was performed using two Agilent PLgel MIXED-B 300 × 7.5 mm columns with 10 μm beads, connected to an Agilent 1260 Series pump, a Wyatt 18-angle DAWN HELEOS light scattering detector, and Optilab rEX differential refractive index detector using THF as the mobile phase. Online determination of dn/dc assumed 100% mass elution under the peak of interest. Size-exclusion chromatography was also performed on a Waters instrument using a refractive index detector and Agilent PL gel 5 μm MiniMIX-D column. THF at 35 °C was used as the mobile phase with a flow rate of 1.0 mL min^{-1}. Molar mass dispersity ($Đ$) was determined against narrow PS standards (Agilent). ^{1}H NMR spectra were collected on a 600 MHz Varian VNMRS. Spectra of

macromonomers and bottlebrushes were collected in $CDCl_3$ and CD_2Cl_2, respectively, at a polymer concentration of 50 – 70 mg mL^{-1} with 128 scans and a pulse delay time of 10 s.

SAXS measurements were performed at beamline 5-ID-D DND-CAT at the Advanced Photon Source (APS) at Argonne National Laboratory (Argonne, Illinois). The beamline was configured with an X-ray wavelength of 0.729 Å. A silver behenate standard was used to calibrate the sample-to-detector distance to 8510 mm. 2D data were reduced by azimuthal averaging to give $I(q)$, where I is intensity in arbitrary units, $q = |\boldsymbol{q}| = 4\pi\lambda^{-1}\sin(\theta/2)$ is the magnitude of the scattering wave vector, λ is the wavelength of incident beam, and θ is the scattering angle.

Self-Consistent Field Theory (SCFT)

The bottlebrush model employed here represents both the side-chains and backbone by continuous Gaussian chains. Previous work has represented the backbone by the more sophisticated worm-like chain model, which was necessary to capture the backbone stiffening that occurs in the large N_{BB} limit.[26] Whereas the worm-like chain model is a defensible assumption when N_{BB} is large, it is less certain that the worm-like chain model is necessary or appropriate when N_{BB} is small because the side-chains will have less stiffening effect on the backbone. Since the behavior of bottlebrushes in the low N_{BB} limit is the emphasis of this paper, the choice was made of continuous Gaussian chains to represent the backbone.

The model was idealized to represent PLA and P4MCL side-chains as Gaussian chains with equivalent degrees of polymerization $N_{SC} \equiv N_{PLA} = N_{P4MCL}$, and the statistical segment lengths of the side-chains and backbone were set to be identical: $b \equiv b_{PLA} = b_{P4MCL} = b_{BB}$. Interactions between PLA and P4MCL side-chains were set to $\chi N_{SC}^{3\,kDa} = 10$, whereas the backbone was considered to be athermal and did not interact enthalpically with either type of side-

chain. These simplifications were made so that our computational analysis of the star-to-bottlebrush transition would be as general as possible and could extend beyond the details of the specific chemistries employed. However, in order to compare the domain spacing between simulations and experiments, we use b_{PLA} = 8 Å (calculated at 30 °C from a polyolefin reference volume of 118 Å^3) as measured by Anderson and Hillmyer.[53] Additional details of the model and simulation methods including a description of our efficient SCFT bottlebrush implementation, the incorporation of dispersity, calculation of $P_{interface}$, and N_{BB} analyses are provided in the Supporting Information.

ASSOCIATED CONTENT

Supporting information that includes detailed experimental procedures, ^{1}H NMR spectra, size-exclusion chromatograms, simulation data, and additional analysis. This material is available free of charge via the Internet at http://pubs.acs.org.

REFERENCES

(1) Bates, C. M.; Bates, F. S. 50th Anniversary Perspective: Block Polymers-Pure Potential. *Macromolecules* **2017**, *50* (1), 3–22.

(2) Bates, F. S.; Fredrickson, G. H. Block Copolymers-Designer Soft Materials. *Phys. Today* **1999**, *52* (2), 32–38.

(3) Bates, F. S.; Hillmyer, M. A.; Lodge, T. P.; Bates, C. M.; Delaney, K. T.; Fredrickson, G. H. Multiblock Polymers: Panacea or Pandora's Box? *Science* **2012**, *336* (6080), 434–440.

(4) Ruzette, A. V.; Leibler, L. Block Copolymers in Tomorrow's Plastics. *Nat. Mater.* **2005**, *4* (1), 19–31.

(5) Kim, H.-C.; Park, S.-M.; Hinsberg, W. D. Block Copolymer Based Nanostructures:

Materials, Processes, and Applications to Electronics. *Chem. Rev.* **2010**, *110* (1), 146–177.

(6) Kataoka, K.; Harada, A.; Nagasaki, Y. Block Copolymer Micelles for Drug Delivery: Design, Characterization and Biological Significance. *Adv. Drug Deliv. Rev.* **2012**, *64* (1), 37–48.

(7) Lin, T.; Chang, A. B.; Luo, S.; Chen, H.; Lee, B.; Grubbs, R. H. Effects of Grafting Density on Block Polymer Self-Assembly: From Linear to Bottlebrush. *ACS Nano* **2017**, *11* (11), 11632–11641.

(8) Sveinbjornsson, B. R.; Weitekamp, R. A.; Miyake, G. M.; Xia, Y.; Atwater, H. A.; Grubbs, R. H. Rapid Self-Assembly of Brush Block Copolymers to Photonic Crystals. *Proc. Natl. Acad. Sci.* **2012**, *109* (36), 14332–14336.

(9) Vatankhah-Varnosfaderani, M.; Keith, A. N.; Cong, Y.; Liang, H.; Rosenthal, M.; Sztucki, M.; Clair, C.; Magonov, S.; Ivanov, D. A.; Dobrynin, A. V.; Sheiko, S. S. Chameleon-like Elastomers with Molecularly Encoded Strain-Adaptive Stiffening and Coloration. *Science* **2018**, *359* (6383), 1509–1513.

(10) Bates, C. M.; Chang, A. B.; Schulze, M. W.; Momčilovic, N.; Jones, S. C.; Grubbs, R. H. Brush Polymer Ion Gels. *J. Polym. Sci. Part B Polym. Phys.* **2016**, *54* (2), 292–300.

(11) Vatankhah-Varnoosfaderani, M.; Daniel, W. F. M.; Zhushma, A. P.; Li, Q.; Morgan, B. J.; Matyjaszewski, K.; Armstrong, D. P.; Spontak, R. J.; Dobrynin, A. V.; Sheiko, S. S. Bottlebrush Elastomers: A New Platform for Freestanding Electroactuation. *Adv. Mater.* **2017**, *29*, 1604209.

(12) Sun, G.; Cho, S.; Clark, C.; Verkhoturov, S. V.; Eller, M. J.; Li, A.; Pavía-Jiménez, A.; Schweikert, E. A.; Thackeray, J. W.; Trefonas, P.; Wooley, K. L. Nanoscopic Cylindrical Dual Concentric and Lengthwise Block Brush Terpolymers as Covalent Preassembled

High-Resolution and High-Sensitivity Negative-Tone Photoresist Materials. *J. Am. Chem. Soc.* **2013**, *135* (11), 4203–4206.

(13) Cheng, L.; Gadelrab, K. R.; Kawamoto, K.; Yager, K. G.; Johnson, J. A.; Alexander-Katz, A.; Ross, C. A. Templated Self-Assembly of a PS-Branch-PDMS Bottlebrush Copolymer. *Nano Lett.* **2018**, *18* (7), 4360–4369.

(14) Fenyves, R.; Schmutz, M.; Horner, I. J.; Bright, F. V.; Rzayev, J. Aqueous Self-Assembly of Giant Bottlebrush Block Copolymer Surfactants as Shape-Tunable Building Blocks. *J. Am. Chem. Soc.* **2014**, *136* (21), 7762–7770.

(15) Lu, X.; Tran, T. H.; Jia, F.; Tan, X.; Davis, S.; Krishnan, S.; Amiji, M. M.; Zhang, K. Providing Oligonucleotides with Steric Selectivity by Brush-Polymer-Assisted Compaction. *J. Am. Chem. Soc.* **2015**, *137* (39), 12466–12469.

(16) Johnson, J. A.; Lu, Y. Y.; Burts, A. O.; Xia, Y.; Durrell, A. C.; Tirrell, D. A.; Grubbs, R. H. Drug-Loaded, Bivalent-Bottle-Brush Polymers by Graft-through ROMP. *Macromolecules* **2010**, *43* (24), 10326–10335.

(17) Iatrou, H.; Hadjichristidis, N. Synthesis of a Model 3-Miktoarm Star Terpolymer. *Macromolecules* **1992**, *25* (18), 4649–4651.

(18) Xie, N.; Li, W.; Qiu, F.; Shi, A. C. σ Phase Formed in Conformationally Asymmetric AB-Type Block Copolymers. *ACS Macro Lett.* **2014**, *3* (9), 909–910.

(19) Shi, W.; Lynd, N. A.; Montarnal, D.; Luo, Y.; Fredrickson, G. H.; Kramer, E. J.; Ntaras, C.; Avgeropoulos, A.; Hexemer, A. Toward Strong Thermoplastic Elastomers with Asymmetric Miktoarm Block Copolymer Architectures. *Macromolecules* **2014**, *47* (6), 2037–2043.

(20) *Miktoarm Star Polymers: From Basics of Branched Architecture to Synthesis, Self-*

Assembly and Applications; Kakkar, A., Ed.; The Royal Society of Chemistry, 2017.

(21) Love, J. A.; Morgan, J. P.; Trnka, T. M.; Grubbs, R. H. A Practical and Highly Active Ruthenium-Based Catalyst That Effects the Cross Metathesis of Acrylonitrile. *Angew. Chem. Int. Ed.* **2002**, *41* (21), 4035–4037.

(22) Roe, R.-J. *Methods of X-Ray and Neutron Scattering in Polymer Science*; Oxford University Press: New York, 2000.

(23) Watts, A.; Kurokawa, N.; Hillmyer, M. A. Strong, Resilient, and Sustainable Aliphatic Polyester Thermoplastic Elastomers. *Biomacromolecules* **2017**, *18* (6), 1845–1854.

(24) Xia, Y.; Olsen, B. D.; Kornfield, J. A.; Grubbs, R. H. Efficient Synthesis of Narrowly Dispersed Brush Copolymers and Study of Their Assemblies: The Importance of Side Chain Arrangement. *J. Am. Chem. Soc.* **2009**, *131* (51), 18525–18532.

(25) Gu, W.; Huh, J.; Hong, S. W.; Sveinbjornsson, B. R.; Park, C.; Grubbs, R. H.; Russell, T. P. Self-Assembly of Symmetric Brush Diblock Copolymers. *ACS Nano* **2013**, *7* (3), 2551–2558.

(26) Dalsin, S. J.; Rions-Maehren, T. G.; Beam, M. D.; Bates, F. S.; Hillmyer, M. A.; Matsen, M. W. Bottlebrush Block Polymers: Quantitative Theory and Experiments. *ACS Nano* **2015**, *9* (12), 12233–12245.

(27) Jha, S.; Dutta, S.; Bowden, N. B. Synthesis of Ultralarge Molecular Weight Bottlebrush Polymers Using Grubbs' Catalysts. *Macromolecules* **2004**, *37* (12), 4365–4374.

(28) Runge, M. B.; Bowden, N. B. Synthesis of High Molecular Weight Comb Block Copolymers and Their Assembly into Ordered Morphologies in the Solid State. *J. Am. Chem. Soc.* **2007**, *129* (34), 10551–10560.

(29) Li, Z.; Ma, J.; Lee, N. S.; Wooley, K. L. Dynamic Cylindrical Assembly of Triblock

Copolymers by a Hierarchical Process of Covalent and Supramolecular Interactions. *J. Am. Chem. Soc.* **2011**, *133* (5), 1228–1231.

(30) Su, L.; Heo, G. S.; Lin, Y.; Dong, M.; Zhang, S.; Chen, Y.; Sun, G.; Wooley, K. L. Syntheses of Triblock Bottlebrush Polymers Through Sequential ROMPs : Expanding the Functionalities of Molecular Brushes. *J. Polym. Sci. Part A Polym. Chem.* **2017**, *55*, 2966–2970.

(31) Xia, Y.; Grubbs, R. H. Efficient Syntheses of Brush Polymers via Living Ring Opening Metathesis Polymerization of Macromonomers. *Macromolecules* **2009**, *50* (2), 197–198.

(32) Lin, T.-P.; Chang, A. B.; Luo, S.-X.; Chen, H.-Y.; Lee, B.; Grubbs, R. H. Effects of Grafting Density on Block Polymer Self-Assembly: From Linear to Bottlebrush. *ACS Nano* **2017**, *11* (11), 11632–11641.

(33) Lin, T. P.; Chang, A. B.; Chen, H. Y.; Liberman-Martin, A. L.; Bates, C. M.; Voegtle, M. J.; Bauer, C. A.; Grubbs, R. H. Control of Grafting Density and Distribution in Graft Polymers by Living Ring-Opening Metathesis Copolymerization. *J. Am. Chem. Soc.* **2017**, *139* (10), 3896–3903.

(34) Kawamoto, K.; Zhong, M.; Gadelrab, K. R.; Cheng, L. C.; Ross, C. A.; Alexander-Katz, A.; Johnson, J. A. Graft-through Synthesis and Assembly of Janus Bottlebrush Polymers from A-Branch-B Diblock Macromonomers. *J. Am. Chem. Soc.* **2016**, *138* (36), 11501–11504.

(35) Widin, J. M.; Schmitt, A. K.; Schmitt, A. L.; Im, K.; Mahanthappa, M. K. Unexpected Consequences of Block Polydispersity on the Self-Assembly of ABA Triblock Copolymers. *J. Am. Chem. Soc.* **2012**, *134* (8), 3834–3844.

(36) Lutz, J.-F.; Ouchi, M.; Liu, D. R.; Sawamoto, M. Sequence-Controlled Polymers. *Science*

2013, *341* (6146), 1238149.

(37) Milner, S. T. Chain Architecture and Asymmetry in Copolymer Microphases. *Macromolecules* **1994**, *27* (8), 2333–2335.

(38) Grason, G. M.; Kamien, R. D. Interfaces in Diblocks: A Study of Miktoarm Star Copolymers. *Macromolecules* **2004**, *37* (19), 7371–7380.

(39) Tselikas, Y.; Iatrou, H.; Hadjichristidis, N.; Liang, K. S.; Mohanty, K.; Lohse, D. J. Morphology of Miktoarm Star Block Copolymers of Styrene and Isoprene. *J. Chem. Phys.* **1996**, *105* (6), 2456–2462.

(40) Shibuya, Y.; Nguyen, H. V. T.; Johnson, J. A. Mikto-Brush-Arm Star Polymers via Cross-Linking of Dissimilar Bottlebrushes: Synthesis and Solution Morphologies. *ACS Macro Lett.* **2017**, *6* (9), 963–968.

(41) Burts, A. O.; Gao, A. X.; Johnson, J. A. Brush-First Synthesis of Core-Photodegradable Miktoarm Star Polymers via ROMP: Towards Photoresponsive Self-Assemblies. *Macromol. Rapid Commun.* **2014**, *35* (2), 168–173.

(42) Golder, M. R.; Nguyen, H. V; Oldenhuis, N. J.; Grundler, J.; Park, E. J.; Johnson, J. A. Brush-First and ROMP-Out with Functional (Macro)Monomers: Method Development, Structural Investigations, and Applications of an Expanded Brush-Arm Star Polymer Platform. *Macromolecules* **2018**, *51* (23), 9861–9870.

(43) Liu, J.; Burts, A. O.; Li, Y.; Zhukhovitskiy, A. V.; Ottaviani, M. F.; Turro, N. J.; Johnson, J. A. "Brush-First" Method for the Parallel Synthesis of Photocleavable, Nitroxide-Labeled Poly(Ethylene Glycol) Star Polymers. *J. Am. Chem. Soc.* **2012**, *134* (39), 16337–16344.

(44) Liao, L.; Liu, J.; Dreaden, E. C.; Morton, S. W.; Shopsowitz, K. E.; Hammond, P. T.; Johnson, J. A. A Convergent Synthetic Platform for Single-Nanoparticle Combination

Cancer Therapy: Ratiometric Loading and Controlled Release of Cisplatin, Doxorubicin, and Camptothecin. *J. Am. Chem. Soc.* **2014**, *136* (16), 5896–5899.

(45) Barnes, J. C.; Bruno, P. M.; Nguyen, H. V. T.; Liao, L.; Liu, J.; Hemann, M. T.; Johnson, J. A. Using an RNAi Signature Assay to Guide the Design of Three-Drug-Conjugated Nanoparticles with Validated Mechanisms, in Vivo Efficacy, and Low Toxicity. *J. Am. Chem. Soc.* **2016**, *138* (38), 12494–12501.

(46) Nguyen, H. V; Chen, Q.; Paletta, J. T.; Harvey, P.; Jiang, Y.; Zhang, H.; Boska, M. D.; Ottaviani, M. F.; Jasano, A.; Rajca, A.; Johnson, J. A. Nitroxide-Based Macromolecular Contrast Agents with Unprecedented Transverse Relaxivity and Stability for Magnetic Resonance Imaging of Tumors. *ACS Cent. Sci.* **2017**, *3* (7), 800–811.

(47) Nguyen, H. V; Detappe, A.; Gallagher, N. M.; Zhang, H.; Harvey, P.; Yan, C.; Mathieu, C.; Golder, M. R.; Jiang, Y.; Ottaviani, M. F.; Jasano, A.; Rajca, A.; Ghobrial, I.; Ghoroghchian, P. P.; Johnson, J. A. Triply Loaded Nitroxide Brush-Arm Star. *ACS Nano* **2018**, *12* (11), 11343–11354.

(48) Nguyen, H. V; Ehrlich, D. C.; Huh, S. J.; Vangamudi, B.; Economides, K. D.; Neenan, A. M.; Ackley, J. C.; Baddour, J.; Paramasivan, S.; Brady, S. W.; Held, E. J.; Reiter, L. A.; Saucier-sawyer, J. K.; Kopesky, P. W.; Chickering, D. E.; Blume-jensen, P.; Johnson, J. A. Reduction of Liver Fibrosis by Rationally Designed Macromolecular Telmisartan Prodrugs. *Nat. Biomed. Eng.* **2018**, *2*, 822–830.

(49) Sowers, M. A.; Mccombs, J. R.; Wang, Y.; Paletta, J. T.; Morton, S. W.; Dreaden, E. C.; Boska, M. D.; Ottaviani, M. F.; Hammond, P. T.; Rajca, A.; Johnson, J. A. Redox-Responsive Branched-Bottlebrush Polymers for in Vivo MRI and Fluorescence Imaging. *Nat. Commun.* **2014**, *5*, 5460.

(50) Dalsin, S. J.; Hillmyer, M. A.; Bates, F. S. Molecular Weight Dependence of Zero-Shear Viscosity in Atactic Polypropylene Bottlebrush Polymers. *ACS Macro Lett.* **2014**, *3* (5), 423–427.

(51) Pesek, S. L.; Li, X.; Hammouda, B.; Hong, K.; Verduzco, R. Small-Angle Neutron Scattering Analysis of Bottlebrush Polymers Prepared via Grafting-through Polymerization. *Macromolecules* **2013**, *46* (17), 6998–7005.

(52) Guo, Z.; Le, A. N.; Feng, X.; Choo, Y.; Liu, B.; Wang, D.; Wan, Z.; Gu, Y.; Zhao, J.; Li, V.; Osuji, C. O.; Johnson, J. A.; Zhong, M. Janus Graft Block Copolymers: Design of Polymer Architecture for Independently Tuned Nanostructures and Polymer Properties. *Angew. Chem. Int. Ed.* **2018**, *57*, 8493–8497.

(53) Anderson, K. S.; Hillmyer, M. A. Melt Chain Dimensions of Polylactide. *Macromolecules* **2004**, *37* (5), 1857–1862.